Revisiting and improving the preparation of silicon-based electrodes for lithium-ion batteries: ball milling impact on poly(acrylic acid) polymer binders

Thibaut Chartrel, Mariama Ndour, Véronique Bonnet, Sébastien Cavalaglio, Luc Aymard, Franck Dolhem, Laure Monconduit, Jean-Pierre Bonnet

Revisiting and improving the preparation of silicon-based electrodes for lithium-ion batteries: ball milling impact on poly(acrylic acid) polymer binders†

Thibaut Chartrel,[abcd] Mariama Ndour,[ab] Véronique Bonnet,[b] Sébastien Cavalaglio,[ad] Luc Aymard,[ad] Franck Dolhem,[bd] Laure Monconduit[cd] and Jean-Pierre Bonnet*[ad]

This study revisits and optimizes silicon/carbon/poly(acrylic acid) – (PAA) composite anode preparation for lithium-ion batteries. The objective is to analyze the specific impact of the high energy ball milling step on the PAA polymer binder and on the composite anode electrochemical behavior in order to improve cycling performance. For this purpose, three commercial PAAs with 15, 450 and 3000 kg mol^{-1} average molar masses are considered. PAA structural alterations induced by ball milling are investigated by SEC, IRTF, ^{1}H NMR and TGA. It appears that PAA 15k is slightly degraded while higher molar mass PAAs are significantly deteriorated. An innovative optimized formulation, combining (1) ball milling of carbon and Si only followed by (2) magnetic stirring of this mixture with PAA and a dispersant is proposed and compared to an all ball milling formulation. The first step is essential to get good electrochemical performance and the second enables the maintenance of polymer integrity. The highest electrochemical capacity retention after 20 cycles is obtained for the PAA 450k-based electrode (84%) compared with those of PAA 15k and PAA 3000k of 62% and 29%, respectively. Interestingly, this capacity retention is also significantly improved compared with that of the corresponding PAA 450k all ball milling formulation electrode (65%).

1. Introduction

Development of new electrochemical technologies for nomadic power storage as well as the optimization of the existing ones is currently a crucial issue. Lithium-ion batteries (LiBs) constitute a largely widespread and advanced power source technology for the actual electrochemical cell market.[1–3] Carbon graphite, the most common negative electrode material (intercalation-type), is characterized by its great electrochemical stability, and a working potential of 0.09 V *vs.* Li^+/Li^0 but a moderate specific capacity of 372 mA h g^{-1}. Some other active materials, especially alloy-type materials such as silicon (Si) or tin (Sn) but also conversion-type materials like metal oxides or hydrides, are under thorough investigation and may be used as substitutes in the near future.[4–7] Si is especially promising because of its high availability, working potential of about 0.40 V *vs.* Li^+/Li^0 and impressive specific capacity of 3579 mA h g^{-1}.[8] This high capacity is related to the $Li_{15}Si_4$ phase obtained during the lithiation process (reaction of 3.75 Li per Si atom)[9] while graphite gives LiC_6 (insertion of only 1 Li for 6 C atoms). This difference is also associated with a huge volume expansion observed in Si (about 280%[10]) to be compared with about 10% only for graphite.[11] This Si expansion is unfortunately responsible for detrimental effects: particle pulverization, electrode particle disconnections and loss of electrical contact resulting in premature capacity fading.[12–14] Another Si expansion side effect is continuous cracks into the solid electrolyte interphase (SEI), resulting in continuous SEI formation and also fast capacity decay.[15–17] As a consequence, studies aim at increasing the Si electrochemical reversibility *via* several ways including, on one side, alloying

[a] *Laboratoire de Réactivité et Chimie des Solides (CNRS UMR 7314), Université de Picardie Jules Verne, 33 Rue Saint Leu, 80039 Amiens Cedex, France. E-mail: jean-pierre.bonnet@u-picardie.fr*

[b] *Laboratoire de Glycochimie, des Antimicrobiens et des Agroressources, (CNRS UMR 7378), Université de Picardie Jules Verne, 33 Rue Saint Leu, 80039 Amiens Cedex, France*

[c] *ICG-AIME, Université Montpellier 2, Bat 15, cc 15-02, Pl. E. Bataillon, 34095 Montpellier cedex 5, France*

[d] *Réseau sur le Stockage Electrochimique de l'Energie (RS2E), CNRS FR3459, 33 Rue Saint Leu, 80039 Amiens Cedex, France*

† Electronic supplementary information (ESI) available: IRTF spectra (ATR) of pristine and of 30 mn SPEX ball milled PAA 15k, PAA 450k and PAA 3000k (Fig. S1) and porosity (%) and active mass loading (mg cm^{-2}) of PAA 15k, PAA 450k and PAA 3000k based electrodes using formulation 1 (a), formulation 2 (b) and formulation 3 (c) (Table S1). See DOI: 10.1039/c8qm00660a

Si alloys or playing with particle shape (use of Si-based alloys,[18–22] Si nanoparticles,[23–26] nanotubes,[27] nanowires[28] and thin layers[29]) and, on the other side, the use of several kinds of polymer binders.[30,31] Moreover, because Si electronic conductivity is not sufficient, electrodes are formulated with conducting carbon for electron transport. Several carbons were thus studied,[32] like "Ketjenblack" or "super P" carbons. The Si negative electrode is consequently a compromise composite structure made of Si, conducting carbon and a polymer binder. Regarding binders, poly(vinylidene fluoride) (PVDF), one of the first investigated Li B anode polymer binders, is not convenient because it only interacts with Si by weak van der Waals forces. This kind of interaction is not strong enough to maintain electrode cohesion and prevent particle disconnections.[33–35] It seems that stronger interactions between Si particles and polymers, like hydrogen bonding or maybe covalent bonding are actually required. Poly(electrolytes) bearing carboxylic acid functions ($COOH/COO^-$) like carboxymethyl cellulose (CMC) and poly(acrylic acid) (PAA) were consequently investigated especially for Si-based anodes, allowing substantial electrode performance enhancement compared to that of PVDF. These conclusions are drawn by many groups such as Koo *et al.* who highlighted capacity retention values of about 1300 mA h g^{-1}, 900 mA h g^{-1} and 100 mA h g^{-1} for, respectively, CMC, PAA and PVDF binder-based silicon electrodes after 100 cycles.[36] Moreover, polymer binder molecular average mass also constitutes an important parameter which was already studied by several groups.[37–40] Briefly, it seems that CMC's molecular weight influences electrochemical performances, with an optimum value, estimated at 700 kg mol^{-1} by Bridel *et al.*[39] Besides, it is important to note that in several laboratory-scale studies from the literature the usual Si/polymer/carbon slurry formulation contains a high-energy ball milling step in the process, using a "Fritsch Pulverisette" or "SPEX" apparatus.[41–45] In complement, in other publications the description of the slurry formulation process remains unclear[46–53] with no precision about polymer ball milling or not. Finally, while the effect of milling was already investigated for Si alone,[54] there is no specific study reported for the polymer binder.

The purpose of this study is to determine the effect of high energy ball milling on poly(acrylic acid) (PAA) and, from there the Si composite electrode's electrochemical properties. The effect of high energy ball milling on the Si particle size was also investigated in complement. It must have indeed a beneficial effect on electrochemical capacity retention.[54] It is here worth noting that many electrode formulation studies from the literature were realized from milled polymer binders without considering eventual binder degradation. For the first time, herein, we take into account the polymer structure evolution impact during the formulation process and thus the molecular mass changes.

2. Experimental section

2.1. Materials

Poly(acrylic acid) sodium salt (PAA-Na) (average molecular weight = 15 000) (PAA 15k) was provided by Sigma Aldrich (USA) and then protonated with an acidic ion exchange resin. Protonation was confirmed by ^{1}H NMR and pH value measurement (not shown here). Poly(acrylic acid) (PAA) (average molecular weight = 450 000) (PAA 450k) and (average molecular weight = 3 000 000) (PAA 3000k) were provided by Sigma Aldrich (USA) and used as received. Silicon powder (Si) was provided by Umicore. It consists of spherical particles with median estimated at about 304 nm. Silicon has an initial SiO_2 content evaluated at 5%. Conducting additive Super C65 carbon (Cc65) was purchased from Timcal. Triton X-100 (Tx_{100}) was purchased from Sigma Aldrich and used as received. Fluoro ethylene carbonate (FEC) was provided by Sigma Aldrich and used as received. LP30 commercial electrolyte (1 M $LiPF_6$ in 1 : 1 w : w ethylene carbonate/dimethyl carbonate, EC/DMC) was purchased from Merck and used as received.

2.2. Characterization techniques

Size exclusion chromatography (SEC) was performed with LB-G 6B, LB-803 and LB-805 columns (Shodex, Germany) using a MALS detector (DAWN 8$^+$ HELEOS II, Wyatt Technology), an RI detector (RID-10A, Shimadzu) and a UV-VIS detector (SPD-20A, Shimadzu). The eluent was a $NaNO_3$/NaN_3 solution (18 g of $NaNO_3$ and 0.6 g of NaN_3 in 1 L of water). Electrode porosity measurements were calculated from a theoretical calculation taking into account the electrode thickness and the different material percentages by weight. Pycnometric densities were performed on an AccuPyc 1330 gas pycnometer using helium gas. Runs were performed 5 times using a 3.5 cm^3 cell. Fourier transformed infrared (FTIR) analyses were done with attenuated total reflection (ATR) mode on a Shimadzu IRAffinity-1S with 4 cm^{-1} resolution, from 400 to 4000 cm^{-1}. Thermo-gravimetric analyses (TGA) were performed under argon flow (50 mL min^{-1}) at a 5 °C min^{-1} temperature ramp on a STA449C Netzsch apparatus coupled to a quadrupole-mass spectrometer (QMS 403 Aeolos). Proton-nuclear magnetic resonance (^{1}H NMR) spectra were recorded at 298 K on a Bruker 400 MHz Avance III HD. PAA samples were placed in D_2O solution in 5 mm NMR tubes. Silicon particle size distributions before (pristine) and after ball milling were estimated with a laser diffraction particle analyzer Mastersizer 3000 (Malvern Instruments, Malvern, U.K.) equipped with a Hydro EV (Malvern Instruments, Malvern, U.K.) dispersion system. This technique permits the determination of particle sizes from 10^{-3} to 3×10^3 µm. The particles were dispersed in a mixture of water and Triton X-100 as dispersing agent (500 µL of 1 wt% of TX-100 in 500 mL of distillated water). The particles were dispersed with an ultrasonic time ratio of 0.1 s pulse/0.1 s rest and with an energy of 96 W and during 90 mn prior to measurement. The Mastersizer 3000 analyzer uses two light sources (red and blue with respective wavelengths of 633 nm and 470 nm) and scattered light intensity angular variation after passing through the wet sample is measured. The obscuration range is 3.02% for Si pristine and 12.69% for ball milled Si.

2.3. Electrochemical studies and electrode preparations

Electrodes were prepared with Si/Cc65/PAA weight% formulation: 70/15/15. In all cases, the total Si/Cc65/PAA total mass was fixed at 600 mg. The three formulations are:

(1) Formulation 1 – usual ball milling formulation: Si, Cc65 and PAA were placed with an adapted quantity of deionized

water in a stainless steel ball mill jar (volume = 50 mL) with 3 stainless steel balls (10 mm of diameter) and subsequently ball milled in a high-energy (SPEX ball mill) milling for 30 minutes at a frequency of 50 Hz. The resulting slurry was then coated on a 15 μm thick structured copper foil. The films were dried at room temperature overnight. Electrode porosity is estimated to be around 60% for 450k and 3000k PAAs and around 65% for 15k PAA.

(2) Formulation 2 – ball milling-free formulation: Si, Cc65, PAA and Tx_{100} (7 mg) were placed in a pill and magnetically stirred with an adapted quantity of deionized water for 120 minutes. The resulting slurry was then coated on a 15 μm thick structured copper foil. The films were dried at room temperature overnight. The electrode porosity was estimated to be around 70%.

(3) Formulation 3 – optimized formulation: Si and Cc65 were placed in a stainless steel ball mill jar (volume = 50 mL) with 3 stainless steel balls (10 mm of diameter). The jar was shaken in a high-energy SPEX ball mill for 30 minutes at a frequency of 50 Hz. PAA, Triton X-100/TX-100 (7 mg) and an adapted quantity of deionized water were then added to the obtained composite powder and magnetically stirred in a pill for 120 minutes. The resulting slurry was then coated on a 15 μm thick structured copper foil. The films were dried at room temperature overnight. Electrode porosity is estimated to be around 70% for both 15k and 450k PAAs and around 60% for 3000k PAA. In all cases, 1 cm^2 disk electrodes were cut and put in an argon-filled glovebox to be assembled into a 2035 coin cell. One glass fiber disk (Whatman GF/D) was placed between the positive (Si/Cc65/PAA electrode) and negative (Li foil) electrodes. The used electrolyte was commercial LP30 (1 M $LiPF_6$ in 1 : 1 w : w ethylene carbonate/dimethyl carbonate, EC/DMC) with 10 wt% added FEC. Cycling was performed with a Mac-Pile (Claix, France) in galvanostatic mode. The cells were cycled between 0.0 and 2.5 V *vs.* Li^+/Li^0 (20 °C) with C/10 (1 Li in 10 h) cycling rate.

3. Results and discussion

3.1. Investigation of polymer binder and silicon particle ball milling impact

SEC-MALS results of pristine and 30 mn ball milled PAA samples are presented in Fig. 1 and the corresponding average molar masses $\bar{M}_n$ and $\bar{M}_w$ and polydispersity index I_p are summarized in Table 1. The highest molar mass commercial PAA, indicated as a 3000 kg mol^{-1} PAA could not be analyzed because of solubility issues (incomplete solubilization). Pristine 15 kg mol^{-1} PAA presents molar masses in the range of the commercial product statement $\bar{M}_n$ = 13 kg mol^{-1} and $\bar{M}_w$ = 27 kg mol^{-1} measured, giving a polydispersity of I_p = 2.03. The pristine 450 kg mol^{-1} PAA molar mass is also close to the expected one but with a higher polydispersity value of I_p = 2.59 ($\bar{M}_n$ = 191 kg mol^{-1} and $\bar{M}_w$ = 495 kg mol^{-1}). We then investigated the impact of SPEX ball milling on the PAA samples. The three PAA samples were ball milled under the same conditions used during the formulation process with ball milling for 30 minutes in deionized water. The samples were then lyophilized to obtain a dry powder and analyzed by ^{1}H NMR, FTIR, TGA and SEC-MALS. From Fig. 1 and Table 1 it can be noted that 450 kg mol^{-1} PAA undergoes a huge average molar mass decrease, from $\bar{M}_n$ = 191 to 65 kg mol^{-1} and $\bar{M}_w$ = 495 to 115 kg mol^{-1} after the ball milling step while the 15 kg mol^{-1} PAA molar mass is not significantly impacted by ball milling with a very small variation from $\bar{M}_n$ = 13 to 10 kg mol^{-1} and $\bar{M}_w$ = 27 to 23 kg mol^{-1}. It is interesting to note here that for the 450 kg mol^{-1} PAA sample the polydispersity decreases from I_p = 2.59 to 1.77, meaning that a more homogeneous size distribution is obtained. On the contrary, for 15k PAA, the polydispersity increases from I_p = 2.08 to 2.30 with ball milling. These apparently contradictory results are in fact in accordance with the work of Smith *et al.* on high-energy mechanical milling of PMMA.[55] These authors demonstrated that, firstly, the ball milling induces a decrease in the PMMA samples' average molar mass and that it follows a kinetics correlated with the molecular mass (the higher the pristine sample's average molar mass, the faster the degradation kinetics). They also show, secondly a polymer sample polydispersity evolution in two steps with an initial broadening followed by a narrowing with the increase of

Table 1 SEC-MALS analysis of pristine and ball milled 15k and 450k PAAs

	Pristine			Ball milled		
	M_w	M_n	I_p	M_w	M_n	I_p
PAA 15 kg mol^{-1}	27	13	2.08	23	10	2.30
PAA 450 kg mol^{-1}	495	191	2.59	115	65	1.77

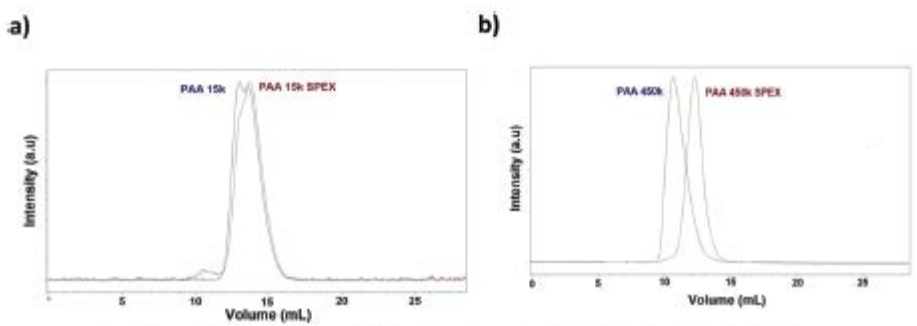

Fig. 1 SEC chromatograms of pristine (blue line) and 30 mn SPEX ball milled (red line) PAA 15k (a) and PAA 450k (b).

milling time duration. From these results it can be concluded in our case, for the same ball milling conditions, that the 450 kg mol^{-1} PAA sample is highly impacted while the 15 kg mol^{-1} PAA sample is less so.

To evaluate more precisely the chemical stability and degradation process of the 3 PAA binders after SPEX ball milling, FTIR, ^{1}H NMR and thermogravimetric analysis (TGA) of the polymers were also performed before and after the 30 minutes ball milling. The FTIR spectra of the pristine and ball milled samples are similar, meaning no noticeable chemical group structure evolution difference in the polymers. All the peaks at 1704 cm^{-1} (C=O stretching), 1455 cm^{-1} (CH_2 deformation), and 1418, 1239 and 1169 cm^{-1} (C–O stretching coupled with O–H)[56] are preserved (Fig. S1, ESI†). ^{1}H NMR spectra of pristine and ball milled PAA samples in D_2O are shown in Fig. 2. All the pristine samples present two groups of peaks, a pseudo-singlet at around 2.42 ppm, attributed to the methine group (–CH) linked to a COOH function and a pseudo-triplet around 1.63, 1.76 and 1.93 ppm attributed to the methylene group ($–CH_2$).[57,58] These signals cannot actually be qualified as singlet and triplet because of the non-equivalency of the protons. The carbon of methine groups –CH corresponds in fact to a pseudochiral center –C*H and the steric arrangement of these pseudoasymmetric centers along the polymer chain is called tacticity and is very well-known for vinylic polymers.[59] In our PAA sample, for the methylene region, the low-field and high-field bands at 1.93 ppm and 1.63 ppm, respectively, are attributed to non-equivalent protons in "m" diads and the middle band at 1.76 ppm corresponds to the "r" diad.[57] The percent of each diad "m" and "r" can be simply calculated here from their corresponding relative intensities. It is very similar in each pristine PAA sample, giving a value of "m" and "r" close to 0.5, *i.e.* probabilities of "r" and "m" configurations of approximately 50% and 50% ("m"/"r" couples of 0.53/0.47; 0.58/0.42; 0.52/0.48 for PAA 15k, 450k and 3000k were, respectively, measured). This result establishes that all 3 commercial samples are atactic, without preferential stereochemical sequences for pseudochiral centers –C*H, *i.e.* totally random polymer chains according to Bernoulian statistics. This result was also established previously for other commercial PAA samples by Chen Chang *et al.*, but with lower molar mass polymers.[58] ^{1}H NMR spectra of ball milled PAA samples are presented in Fig. 2. 15k ball milled PAA NMR shows an unmodified response with respect to the pristine one (Fig. 2a). Concerning 450k and 3000k PAAs, a significant signal enlargement can be observed at the same time for methine –CH and methylene $–CH_2$ protons (Fig. 2b and c). This growth is due to an increase of the chemical environment diversity caused by some polymer backbone breaks leading to smaller fragments. These observations can be quantified by an increase of signal width at half height values. Taking the methine –CH group as a reference, the 15k PAA width at half height increases by 0.83 Hz while those of PAA 450k and 3000k PAAs increase, by 179 Hz and 14 Hz, respectively, after ball milling. These results indicate that the different PAAs are not equally degraded, with a higher degradation ratio for 450k PAA than for 3000k PAA. 15k PAA appears to be less affected. This is coherent with our previous SEC study, showing that the PAA 15k is less degraded by ball milling compared with PAA 450k. TGA thermograms at a 5 °C min^{-1} rate under argon for both pristine and ball milled PAA samples are shown in Fig. 3. PAA samples actually decompose in 3 successive steps, according to the literature.[60,61] The first weight loss corresponds to absorbed water emission and occurs until 95 °C. This loss represents between 4 and 9% of the total mass. The second loss of mass is attributed to a dehydration step. Reported with a starting temperature ($T^{\circ}_{onset}2$) between 141 °C[60] and 170 °C[61] and with a maximum at about 250 °C; it corresponds to water loss from carboxylic acids, leading to anhydride group formation. This mass loss corresponds to around 23% weight. The last step (51% of mass loss), starts from 300 °C ($T^{\circ}_{onset}3$) and is associated with decarboxylation and polymer chain scissions.[61] The resulting mass is finally reported to be close to 17% at 500 °C.[60] All our pristine and ball milled samples are following this degradation process. More precisely, in our PAA samples (Fig. 3a–c), all the ball milled ones systematically present lower $T^{\circ}_{onset}2$ and $T^{\circ}_{onset}3$ compared to the pristine samples. For PAA 15k $T^{\circ}_{onset}2 = 164$ °C before and 117 °C after ball milling, for PAA 450k $T^{\circ}_{onset}2 = 155$ °C before and 148 °C after and for PAA 3000k $T^{\circ}_{onset}2 = 145$ °C before and 141 °C after. For $T^{\circ}_{onset}3$ it decreases from 284 °C to 235 °C for PAA 15k, from 301 °C to 296 °C for PAA 450k and from 316 °C to 293 °C for PAA 3000k. This T°_{onset} decrease means actually that ball milling leads to some polymer structure alterations and therefore facilitates decomposition. This observation is in accordance

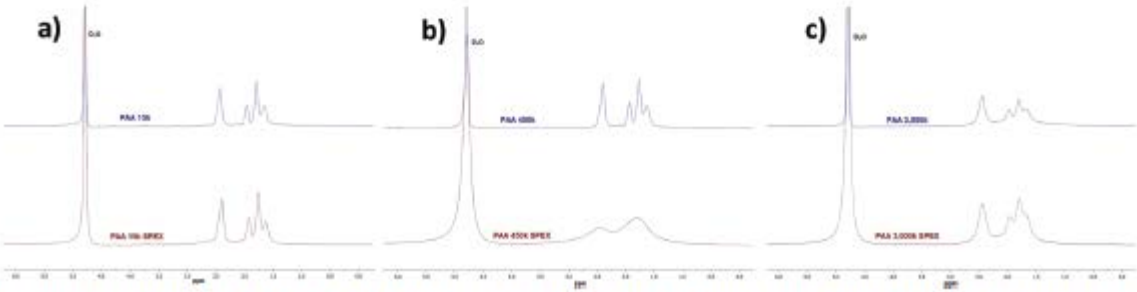

Fig. 2 ^{1}H NMR spectra of pristine (blue line) and 30 mn SPEX ball milled (red line) PAA 15k (a), PAA 450k (b) and PAA 3000k (c) solutions in D_2O.

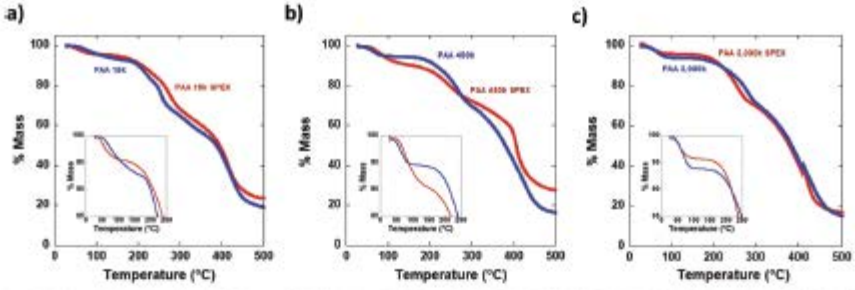

Fig. 3 TGA curves of of pristine (blue line) and 30 mn SPEX ball milled (red line) PAA 15k (a), PAA 450k (b) and PAA 3000k (c) (argon, heating rate 5 °C min^{-1}, insets: close-up until 250 °C).

with work of Castricum *et al.*[62] and also in accordance with our SEC and NMR results. TGA analyses show then that ball milling drastically reduces the properties of 450k PAA while 15k and 3000k PAAs seem to be less damaged by this milling step.

Besides, silicon particle degradation by ball milling is studied by a laser diffraction analyzer and the results are presented in Fig. 4. A multimodal distribution with three Si particle populations around 30 nm, 380 nm and 3.34 μm and respective percentages of 47.00%, 43.55% and 9.45% are found for pristine silicon. After ball milling, these populations are conserved (respectively, 30 nm, 340 nm and 4.31 μm) but the particles' respective percentages are quite modified (14.44%, 23.61% and 35.50%, respectively). Moreover, a 4th population at 33.20 μm, corresponding to 26.45%, appears. This morphology change (global average particle size increase after ball milling) corresponds to a clustering of silicon particles, with agglomerates constituted of sub-micrometric particles welded together. This phenomenon was previously observed by Gauthier *et al.*[54] for Si particles of 1 to 5 μm after 20 h of SPEX ball milling. It must be noted that this Si particle ball milling is beneficial for electrochemistry with better capacity retention attributed to a nano-structuration phenomenon, creating grain boundaries where faster Li diffusion may happen.[54]

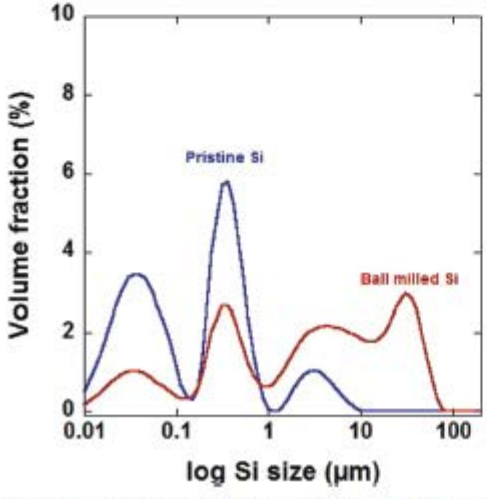

Fig. 4 Particle size distribution analyses of pristine silicon (blue line) and 30 mn SPEX ball milled silicon (red line) powders.

3.2. Electrochemical characterization

The three different PAA chain length samples in their acidic form were first used as binders in silicon-based composite electrodes following a formulation including polymer ball milling (formulation 1, see Experimental part). A silicon/carbon/polymer mixture (Si/Cc65/PAA) (70/15/15 wt%) was electrochemically tested against lithium metal (half cell) using liquid electrolyte LP30 with 10 wt% added FEC (see Experimental part). The corresponding electrochemical results (potential (V) *versus* specific capacity curves (mA h g^{-1} of Si)) are shown in Fig. 5. The active mass loadings (in mg cm^{-2}) are, respectively, 1.19 for PAA 15k and 450k and 1.05 for PAA 3000k electrodes and the electrode porosities are estimated to be about 60% for PAA 450k and 3000k electrodes (65% for PAA 15k) (Table S1, ESI†). In complement, Table 2 summarizes some electrochemical characteristics (1st charge capacity (mA h g^{-1}), 1st cycle coulombic efficiency (CE) (%), 20th charge capacity (mA h g^{-1}), 20th charge capacity/1st charge capacity (%), and polarization 1st cycle/20th cycle (V)). First, the 450 kg mol^{-1} PAA-based cell presents a better CE at the first cycle compared to 3000k and 15k PAA cells (85% for 450k PAA *versus* 79% and 68%, respectively for 3000k and 15k PAA). Better capacity retention at the twentieth cycle is also observed for the 450 kg mol^{-1} PAA-based cell, with a charge capacity of 2126 mA h g^{-1}, to be compared with 960 and 384 for 3000k and 15k PAA cells, respectively (Fig. 5b). Polarization curves, which correspond to the difference between the potential of the $(n + 1)$ charge and of the (n) discharge, were also estimated for all cases. Both 15k and 3000k PAA galvanostatic curves undergo a polarization increase from 0.34 V at the first cycle to 1.05 and 0.86 V at the twentieth cycle while 450k PAA's polarization decreases from 0.34 to 0.30 V under the same conditions (Fig. 5c). These observations are in accordance with a study of Hu *et al.*[37] on graphite rich silicon/graphite composite anodes for lithium ion batteries using PAA as a binder. These authors show that silicon/graphite-based electrodes with PAAs with an average molecular mass number $\bar{M}_n \approx 150$ kg mol^{-1} present better performances compared to that using smaller PAA, with higher capacities of 343 and

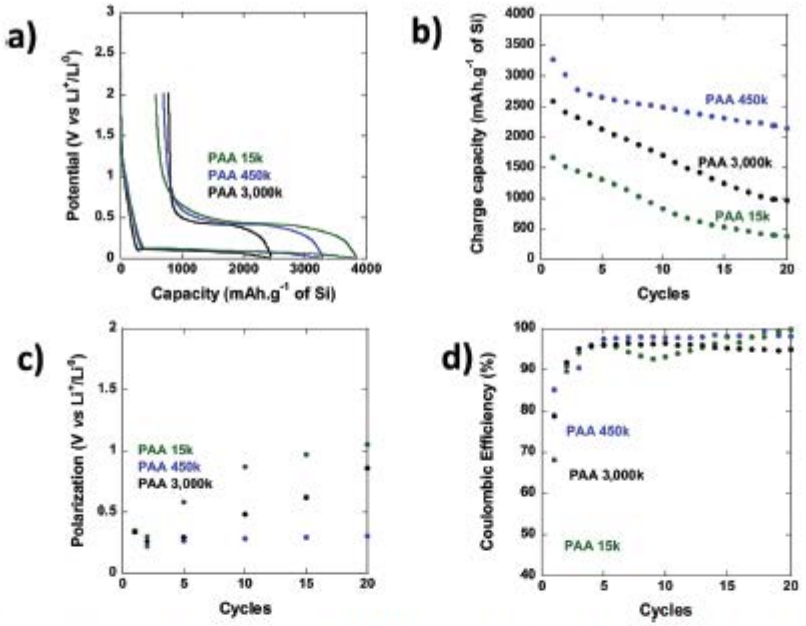

Fig. 5 First galvanostatic cycle profile (a), evolution of charge capacity with cycle curves (b), polarization evolution curves (c) and coulombic efficiency variation (d) of Si/Cc65/binder electrodes (70/15/15 wt%) with formulation 1 using PAA 15k (green line), PAA 450k (blue line) and PAA 3000k (black line) (20 °C, C/10 (1 Li in 10 hours), LP30 + FEC (10 v%), *versus* Li^+/Li^0).

Table 2 Cell characteristics of 15k, 450k and 3000k PAA-based electrodes using formulation 1 and the 450k PAA silicon-based electrode using formulation 2

Formulation 1	PAA 15k	PAA 450k	PAA 3000k	Formulation 2 PAA 450k
1st charge (mA h g^{-1})	1669	3270	2594	3456
1st cycle CE (%)	68	85	79	76
20th charge (mA h g^{-1})	384	2126	960	170
20th charge/1st charge (%)	23	65	37	5
Polarization 1st cycle/20th cycle (V)	0.35/1.05	0.34/0.30	0.34/0.86	0.28/1.51

322 mA h g^{-1} after 100 cycles for $\bar{M}_n$ = 147 and 167 kg mol^{-1} PAAs respectively and of 278 and 224 mA h g^{-1} for $\bar{M}_n$ < 24 kg mol^{-1} PAAs. The given explanation is that PAA smaller than 150 kg mol^{-1} may not be able to maintain the ester bonding between the binder and siloxyl groups, leading to some cohesion loss and cracks. It can otherwise be thought, based on the PAA pelota conformation[41] that a high molar mass PAA will more isolate electronically Si and additive carbon.

Starting from the observation of polymer binder degradation during ball milling and in order to investigate the ball milling impact on cycling performance, a formulation without ball milling was considered (formulation 2 – SPEX-free). Therefore, Si, carbon, polymer binder, and Tx_{100} dispersant were magnetically stirred in deionized water for 2 hours and then cast on a copper foil before drying, as previously described. The resulting electrodes were cycled in a coin cell *versus* Li^+/Li^0 and the active mass loading (in mg cm^{-2}) is 1.47 (Table S1, ESI†). This highly porous electrode (porosity is estimated around 70% – Table S1, ESI†, slightly higher than that with formulation 1) shows a 1st cycle CE of 76%, and a capacity of 3456 mA h g^{-1} and 170 mA h g^{-1} for 1st and 20th charges, respectively. The observed polarization was 0.28 and 1.51 V at the 1st cycle and 20th cycle, respectively (Fig. 6). Here, fast capacity fading is observed and can be attributed to the absence of energetic silicon ball milling and good mixing with carbon and PAA binder. Several reasons could be evoked for these low performances without silicon/carbon ball milling. First, energetic ball milling creates micro or nano-cracks and defects, *i.e.* reactive sites, and modifies the surface energy. All these phenomena enhance the electrochemical reactivity.[63] Secondly, the absence of reduction of the oxidized Si surface, which can be induced by the additive carbon during energetic ball milling, could also be suggested to be the origin of these low performances. The low cyclability is correlated with an important polarization increase (from 0.28 V at the 1st cycle to 1.51 V at the 20th). Moreover, as previously underlined, a silicon planetary ball milling induces actually a silicon nano-structuration thanks to grain boundary creation with, consequently, a better electrochemical cyclability for micrometer silicon.[54] This nano-

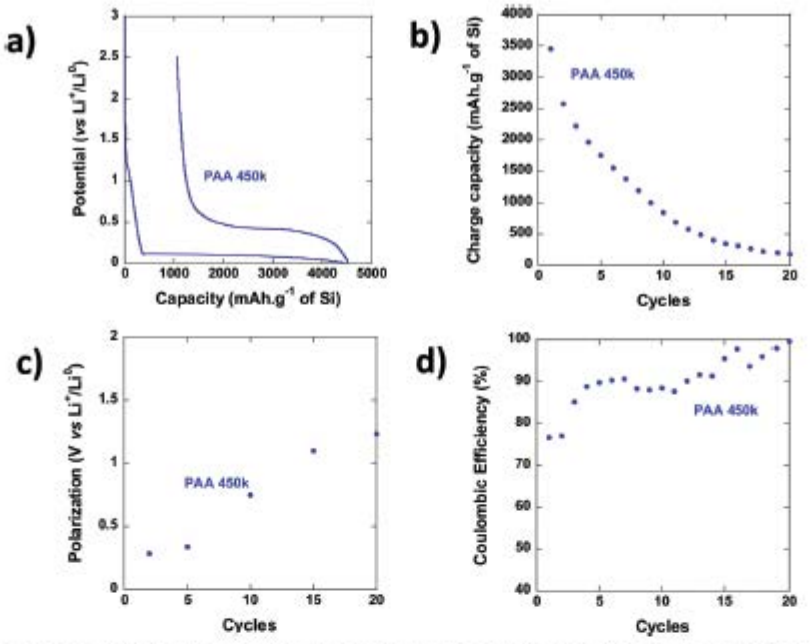

Fig. 6 First galvanostatic cycle profile (a), evolution of charge capacity with cycle curves (b), polarization evolution curves (c) and coulombic efficiency variation (d) of Si/Cc65/binder electrodes (70/15/15 wt%) with formulation 2 using PAA 450k (blue line) (20 °C, C/10 (1 Li in 10 hours), LP30 + FEC (10 v%), *versus* Li^+/Li^0).

structuration phenomenon, missing in our formulation 2 could finally also explain these weak performances.

Based on the two previous formulation results, we developed here an innovative formulation combining both energetic silicon milling and PAA stirring (formulation 3). This new process consists, first of SPEX dry ball milling of silicon and additive carbon, followed by an addition of PAA binder stirred with deionized water and dispersant to homogenize the slurry. The resulting 70/15/15 wt% slurry (Si/Cc65/PAA) was electrochemically characterized *versus* Li^+/Li^0, as previously described. The results are presented in Fig. 7 and summarized in Table 3. This new optimized formulation induces an electrochemical cyclability improvement for 15k and 450k PAAs. Indeed, a significant increase of the charge capacity retention from 23% to 62% is observed at the 20th cycle for 15k PAA and from 62% to 84% for 450k PAA with formulation 3 compared with that of the previous "ball milling" formulation 1. These cells exhibit charge capacities at the 20th cycle of 2023 mA h g^{-1}, 2957 mA h g^{-1} and 853 mA h g^{-1}, respectively, for PAA 15k, 450k and 3000k. Besides, electrode porosities are estimated at about 70% for PAA 450k and 3000k electrodes (65% for PAA 15k) against 60% in the usual SPEX formulation for PAA 450k and 3000k electrodes (65% for PAA 15k) – (Table S1, ESI†). The active mass loading values (in mg cm^{-2}) are, respectively, 1.12 for PAA 15k and 450k and 1.26 for PAA 3000k electrodes (Table S1, ESI†). Moreover, the 15k and 450k PAA electrode polarization values remain almost constant along the first 20 cycles with a respective limited increase of 0.02 and 0.03 V, whereas an increase from 0.34 to 0.52 V is observed for the 3000k PAA. The later clearly shows lower performances. Fig. 7 also shows that the coulombic efficiency (CE) is improved for the 450k PAA-based electrode in this formulation 3, compared to the 15k- and 3000k-based electrodes. A value of about 95% is then reached at the 2nd cycle, higher than the 15k (84.5%) and 3000k (73%)-based electrodes values, at the same cycle.

SEM pictures of 450k PAA Si pristine electrodes of formulation 1 and 3 are presented in Fig. 8a and c. A significant morphological difference can be noticed here between the two formulations. The composite electrode formed of the 450k ball milling formulation presents a homogeneous surface with some noticeable cracks. In contrast, the optimized composite electrode presents a more complex morphology, without noticeable cracks and with a higher apparent porosity. These features would likely lead to better lithium/electron diffusion and consequently better electrochemical behavior. Formulation 1 and 3 washed post-mortem electrodes after 20 cycles (Fig. 8b and d) exhibit a more compact surface with a global apparent porosity decrease. This observation is particularly true for the formulation 1 electrode which appears more impervious while the optimized electrode still presents some porosity. Such phenomena may be attributed to the SEIs which fill the pores of the electrode (formulation 1) and increase the resistivity to ions and electrons and decrease the performance while the optimized electrode (formulation 3) benefits from a better SEI structure allowing better performance. For comparison for both 450k- and 15k-based electrodes, the polarization is quite constant during the first 20 cycles (0.30 V for formulation 1

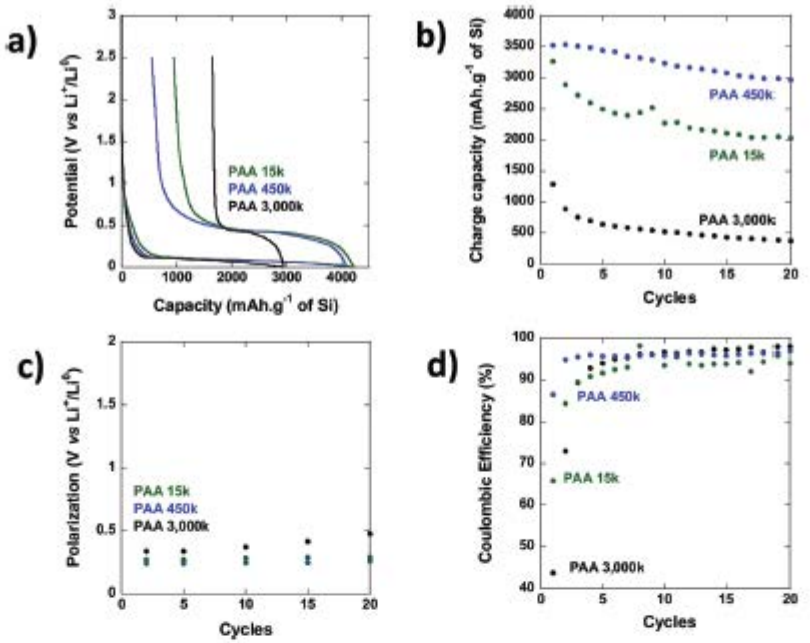

Fig. 7 First galvanostatic cycle profile (a), evolution of charge capacity with cycle curves (b), polarization evolution curves (c) and coulombic efficiency variation (d) of Si/Cc65/binder electrodes (70/15/15 wt%) with formulation 3 using PAA 15k (green line), PAA 450k (blue line) and PAA 3000k (black line) (20 °C, C/10 (1 Li in 10 hours), LP30 + FEC (10 v%), *versus* Li^+/Li^0).

Table 3 Cell characteristics of 15k, 450k and 3000k PAA-based electrodes using formulation 3

Formulation 3	PAA 15k	PAA 450k	PAA 3000k
1st charge (mA h g^{-1})	3263	3520	2941
1st cycle CE (%)	66	86	44
20th charge (mA h g^{-1})	2023	2957	853
20th charge/1st charge (%)	62	84	29
Polarization 1st cycle/20th cycle (V)	0.27/0.29	0.24/0.27	0.34/0.52

against 0.27 V for formulation 3). The retention of binder integrity can be therefore evoked as responsible for this improvement. The absence of binder degradation involves a higher polymer average molar mass compared to that of its milled counterpart and induces, as a consequence, better interactions between electrode components, especially silicon. In this sense, this average molecular mass retention is favorable for 15 and 450 kg mol^{-1} PAA. On the contrary, in the case of the 3000 kg mol^{-1} PAA-based cell, the composite electrode suffers from the polymer critical molar mass and restricted electrochemical performances are observed, regardless of whether formulation 1 or 3 is used. It must be highlighted here that a relatively comparable PAA ($\bar{M}_n$ = 167 kg mol^{-1} and $\bar{M}_w$ = 964 kg mol^{-1}) gave also the best results in a very recent study of Hu *et al.*[37] on graphite rich silicon composite electrodes for Li-ion batteries. The higher initial specific capacity and higher average capacity over 100 cycles is indeed obtained for an electrode based on this polymer, compared to lower mass PAA-based electrodes. More widely, these authors suggest that a $\bar{M}_n$ range of 24 to 150 kg mol^{-1} permits optimized performance to be achieved. Here, this assertion can be confirmed in our case, with clear evidence that a PAA of $\bar{M}_n$ = 13 kg mol^{-1} and $\bar{M}_w$ = 27 kg mol^{-1} gives lower performances. Interestingly, in complement to the study of Hu *et al.*, we demonstrated here that a higher average molar mass PAA (3000 kg mol^{-1}) also gives lower performance. This effect is probably linked to the limited solubility of this high molar mass PAA, limiting its dispersion in solution/electrolyte and, therefore, limiting its possibility to create covalent links to SiOH groups on the surface of Si. Furthermore, it must be highlighted here that in the study of Hu *et al.* the electrode intrinsic capacity is much lower than in our case due to the low % of Si in the composite. There, 15% of Si gives a maximum theoretical initial capacity of 854 mA h g^{-1} for the composite electrode. This value has to be compared to our maximum theoretical initial capacity of 3589 mA h g^{-1} for a composite electrode using only silicon as the active material. Here, in our best result (formulation 3 with PAA 450k) the initial charge capacity of 3520 mA h g^{-1} is decreased to 2957 mA h g^{-1} for the 20th charge. Besides, another consequence of this low Si% in the study of Hu *et al.* is that the electrode volume expansion during electrochemical cycling (breathing) is much lower than in our case, giving a much easier manageable electrode, especially with intrinsic better reversibility. Overall, a question can be asked here on the polymer binder impact in regard to the inherent active material capacity. In our opinion, this effect is easier to highlight if the electroactive material capacity is high, *i.e.* with a Si rich electrode rather than with a carbon rich electrode. Nevertheless, in the latter case discrepancies are higher.

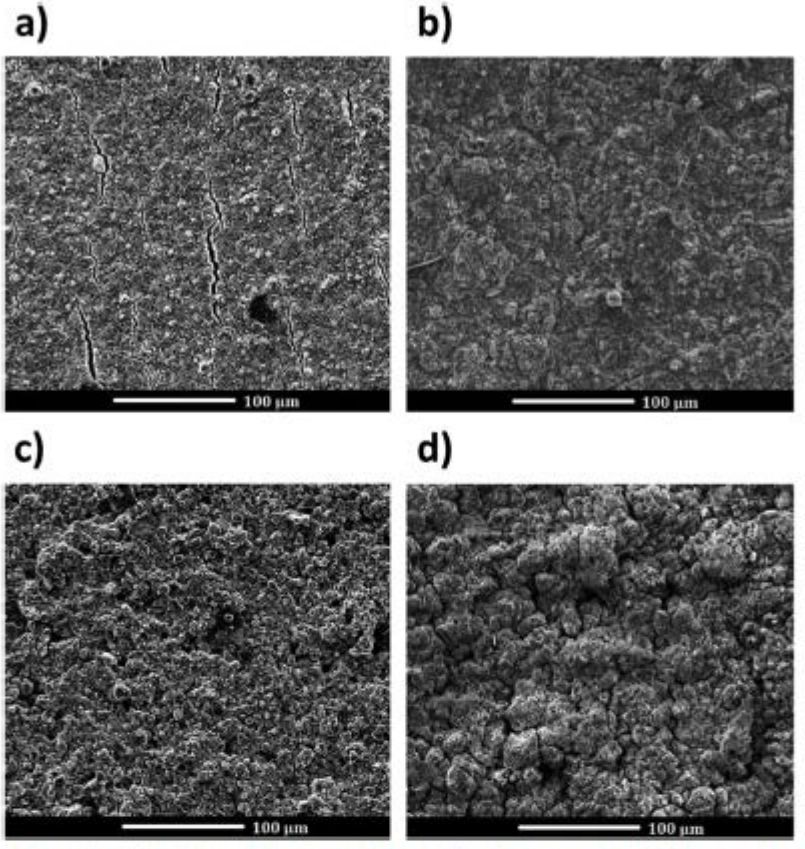

Fig. 8 SEM micrographs of the pristine 450k PAA-based formulation 1 electrode (a) and the same after the 20th charge (b) and the pristine 450k PAA-based formulation 3 electrode (c) and the same after the 20th charge (d).

4. Conclusions

The detrimental effect of the energetic ball milling step on PAA binders used for Si-based electrode preparation and its strong impact on performance was demonstrated here for the first time. Several characterizations realized on pre- and post-ball milled PAA of three different commercial samples (PAA 15k, 450k, 3000k) support this statement (SEC study, ^{1}H NMR, TGA analysis). SEC-MALS analysis proved that the average molecular masses decrease for PAA 15k and 450k, especially for PAA 450k; ^{1}H NMR demonstrates a resolution loss for all samples attributed to an increase of the different chemical environments and linked to chain degradation, especially for PAA 450k. FTIR study does not show any difference between all pristine and ball milled polymers, meaning that there are no clearly noticeable chemical function changes. Finally, TGA study demonstrates a lower thermal stability for all PAA samples after ball milling. More precisely, the small polymer sample (PAA 15k) is not affected by energetic ball milling while higher molar mass PAAs (PAA 450k and 3000k) suffer from this energetic milling step. Degradation seems to be maximum for PAA 450k. Here, we also introduce an optimized formulation, with a wet ball milling of only carbon and Si, this last step being necessary to get a homogeneous electrode able to give satisfactory performance. Increases of capacity retention at the 20th cycle were observed with this optimized formulation, going from 65 to 84% and from 23 to 62%, respectively, for 450k and 15k PAA-based composite anodes. PAA 3000k possesses limited solubility in solvents, which limits (i) its dispersion in the slurry and (ii) therefore its possibility to bond SiOH groups of Si particle surfaces and (iii) the performance in the battery. In addition, we confirm that polymer binder average molecular mass constitutes an important parameter regarding the Si-based electrode cyclability. There is no doubt that this conclusion may be extended to other p-block element-based electrodes.[37–40] Here, we suggest that the PAA optimal average molecular mass for a rich silicon-based anode (70%) is close to $\bar{M}_n$ = 191 kg mol^{-1} and $\bar{M}_w$ = 495 kg mol^{-1} (PAA 450k), since lower performances have been obtained with lower or higher PAA average molar masses (PAA 15k and 3000k). These results can be compared to the study of Hu *et al.*[37] who estimated the optimum PAA with average masses of $\bar{M}_n$ = 167 kg mol^{-1} and $\bar{M}_w$ = 964 kg mol^{-1}. Nevertheless, it must be highlighted that this last study was realized with a graphite rich silicon composite electrode (15% of Si).

Conflicts of interest

The authors declare there are no conflicts of interest for this manuscript.

Acknowledgements

Financial support from the European Union – FEDER (Fonds Européen de Développement Régional), from the CNRS, from the Région Picardie and from the RS2E (Réseau sur le Stockage Electrochimique de l'Energie FR CNRS 3459) for the PENSA research project is gratefully acknowledged. The authors also deeply thank D. Cailleux and M. Courty for NMR and TGA experiments and "Platform of Electronic Microscopy" for help in SEM characterization.

Notes and references

1 J. M. Tarascon and M. Armand, *Nature*, 2001, **414**, 359–367.
2 N.-S. Choi, Z. Chen, S. A. Freunberger, X. Ji, Y.-K. Sun, K. Amine, G. Yushin, L. F. Nazar, J. Cho and P. G. Bruce, *Angew. Chem., Int. Ed.*, 2012, **51**, 9994–10024.
3 B. Dunn, H. Kamath and J.-M. Tarascon, *Science*, 2011, **334**, 928–935.
4 J. Swiatowska and P. Barboux, *Lithium Process Chemistry*, Elsevier, 1st edn, 2015, pp. 137–149.
5 Y. Huang, X. Huang, J. Lian, D. Xu, L. Wang and X. Zhang, *J. Mater. Chem.*, 2012, **22**, 2844–2847.
6 X. Huang, R. Wang, D. Xu, Z. Wang, H. Wang, J. Xu, Z. Wu, Q. Liu, Y. Zhang and X. Zhang, *Adv. Funct. Mater.*, 2013, **23**, 4345–4353.
7 L. Aymard, Y. Oumellal and J.-P. Bonnet, *Beilstein J. Nanotechnol.*, 2015, **6**, 1821–1839.
8 U. Kasavajjula, C. Wang and A. J. Appleby, *J. Power Sources*, 2007, **163**, 1003–1039.
9 M. N. Obrovac and L. Christensen, *Electrochem. Solid-State Lett.*, 2004, **7**, A93–A96.
10 T. D. Hatchard and J. R. Dahn, *J. Electrochem. Soc.*, 2004, **151**, A838–A842.
11 J. Tirado, *Mater. Sci. Eng., R*, 2003, **40**, 103–136.
12 C. K. Chan, H. Peng, G. Liu, K. McIlwrath, X. F. Zhang, R. A. Huggins and Y. Cui, *Nat. Nanotechnol.*, 2008, **3**, 31–35.
13 C. Chen, S. H. Lee, M. Cho, J. Kim and Y. Lee, *ACS Appl. Mater. Interfaces*, 2016, **8**, 2658–2665.
14 K. Feng, M. Li, W. Liu, A. G. Kashkooli, X. Xiao, M. Cai and Z. Chen, *Small*, 2018, **14**, 1702737.
15 Z.-H. Wu, J.-Y. Yang, B. Yu, B.-M. Shi, C.-R. Zhao and Z.-L. Yu, *Rare Met.*, 2016, 1–8.
16 K. W. Schroder, H. Celio, L. J. Webb and K. J. Stevenson, *J. Phys. Chem. C*, 2012, **116**, 19737–19747.
17 J. Zhu, T. Wang, F. Fan, L. Mei and B. Lu, *ACS Nano*, 2016, **10**, 8243–8251.
18 J. Wang, T. Xu, X. Huang, H. Li and T. Ma, *RSC Adv.*, 2016, **6**, 87778–87790.
19 T. D. Bogart, X. Lu, M. Gu, C. Wang and B. A. Korgel, *RSC Adv.*, 2014, **4**, 42022–42028.
20 D. Ma, Z. Cao and A. Hu, *Nano-Micro Lett.*, 2014, **6**, 347–358.
21 X. Zuo, J. Zhu, P. Müller-Buschbaum and Y.-J. Cheng, *Nano Energy*, 2017, **31**, 113–143.
22 J. K. Lee, C. Oh, N. Kim, J.-Y. Hwang and Y.-K. Sun, *J. Mater. Chem. A*, 2016, **4**, 5366–5384.
23 H. Li, X. Huang, L. Chen, Z. Wu and Y. Liang, *Electrochem. Solid-State Lett.*, 1999, **2**, 547–549.
24 H. Tian, F. Xin, X. Wang, W. He and W. Han, *J. Materiomics*, 2015, **1**, 153–169.
25 X. H. Liu, L. Zhong, S. Huang, S. X. Mao, T. Zhu and J. Y. Huang, *ACS Nano*, 2012, **6**, 1522–1531.
26 X. H. Liu and J. Y. Huang, *Energy Environ. Sci.*, 2011, **4**, 3844.
27 M.-H. Park, M. G. Kim, J. Joo, K. Kim, J. Kim, S. Ahn, Y. Cui and J. Cho, *Nano Lett.*, 2009, **9**, 3844–3847.
28 C. K. Chan, H. Peng, G. Liu, K. McIlwrath, X. F. Zhang, R. A. Huggins and Y. Cui, *Nat. Nanotechnol.*, 2008, **3**, 31–35.
29 T. Takamura, S. Ohara, M. Uehara, J. Suzuki and K. Sekine, *J. Power Sources*, 2004, **129**, 96–100.
30 B. Lestriez, *C. R. Chim.*, 2010, **13**, 1341–1350.
31 N.-S. Choi, S.-Y. Ha, Y. Lee, J. Y. Jang, M.-H. Jeong, W. C. Shin and M. Ue, *J. Electrochem. Sci. Technol.*, 2015, **6**, 35–49.
32 F. Beguin and E. Frackowiak, *Carbons for Electrochemical Energy Storage and Conversion Systems*, CRC Press, 1st edn, 2010, p. 263.
33 M. Yoo, C. W. Frank, S. Mori and S. Yamaguchi, *Chem. Mater.*, 2004, **16**, 1945–1953.
34 M. Yoo, C. W. Frank and S. Mori, *Chem. Mater.*, 2003, **15**, 850–861.
35 M. Yoo, C. W. Frank, S. Mori and S. Yamaguchi, *Polymer*, 2003, **44**, 4197–4204.
36 B. Koo, H. Kim, Y. Cho, K. T. Lee, N.-S. Choi and J. Cho, *Angew. Chem., Int. Ed.*, 2012, **51**, 8762–8767.
37 B. Hu, I. A. Shkrob, S. Zhang, L. Zhang, J. Zhang, Y. Li, C. Liao, Z. Zhang, W. Lu and L. Zhang, *J. Power Sources*, 2018, **378**, 671–676.
38 H.-K. Park, B.-S. Kong and E.-S. Oh, *Electrochem. Commun.*, 2011, **13**, 1051–1053.
39 J.-S. Bridel, T. Azaïs, M. Morcrette, J.-M. Tarascon and D. Larcher, *Chem. Mater.*, 2010, **22**, 1229–1241.
40 B.-R. Lee and E.-S. Oh, *J. Phys. Chem. C*, 2013, **117**, 4404–4409.
41 Z. Karkar, D. Guyomard, L. Roué and B. Lestriez, *Electrochim. Acta*, 2017, **258**, 453–466.
42 C. R. Hernandez, A. Etiemble, T. Douillard, D. Mazouzi, Z. Karkar, E. Maire, D. Guyomard, B. Lestriez and L. Roué, *Adv. Energy Mater.*, 2017, **8**, 1701787.
43 J. Guo and C. Wang, *Chem. Commun.*, 2010, **46**, 1428–1430.
44 A. Tranchot, H. Idrissi, P. X. Thivel and L. Roué, *J. Electrochem. Soc.*, 2016, **163**, A1020–A1026.
45 M. Murase, N. Yabuuchi, Z.-J. Han, J.-Y. Son, Y.-T. Cui, H. Oji and S. Komaba, *ChemSusChem*, 2012, **5**, 2307–2311.
46 Z.-J. Han, K. Yamagiwa, N. Yabuuchi, J.-Y. Son, Y.-T. Cui, H. Oji, A. Kogure, T. Harada, S. Ishikawa, Y. Aoki and S. Komaba, *Phys. Chem. Chem. Phys.*, 2015, **17**, 3783–3795.
47 Z.-Y. Wu, L. Deng, J.-T. Li, Q.-S. Huang, Y.-Q. Lu, J. Liu, T. Zhang, L. Huang and S.-G. Sun, *Electrochim. Acta*, 2017, **245**, 371–378.

48 D. Liu, Y. Zhao, R. Tan, L.-L. Tian, Y. Liu, H. Chen and F. Pan, *Nano Energy*, 2017, **36**, 206–212.
49 S. Lim, H. Chu, K. Lee, T. Yim, Y.-J. Kim, J. Mun and T.-H. Kim, *ACS Appl. Mater. Interfaces*, 2015, **7**, 23545–23553.
50 L. Lü, H. Lou, Y. Xiao, G. Zhang, C. Wang and Y. Deng, *RSC Adv.*, 2018, **8**, 4604–4609.
51 C. C. Nguyen, T. Yoon, D. M. Seo, P. Guduru and B. L. Lucht, *ACS Appl. Mater. Interfaces*, 2016, **8**, 12211–12220.
52 J. Lopez, Z. Chen, C. Wang, S. C. Andrews, Y. Cui and Z. Bao, *ACS Appl. Mater. Interfaces*, 2016, **8**, 2318–2324.
53 T. Ikonen, T. Nissinen, E. Pohjalainen, O. Sorsa, T. Kallio and V.-P. Lehto, *Sci. Rep.*, 2017, **7**, 7880.
54 M. Gauthier, D. Mazouzi, D. Reyter, B. Lestriez, P. Moreau, D. Guyomard and L. Roué, *Energy Environ. Sci.*, 2013, **6**, 2145–2155.
55 A. P. Smith, J. S. Shay, R. J. Spontak, C. M. Balik, H. Ade, S. D. Smith and C. C. Koch, *Polymer*, 2000, **41**, 6271–6283.
56 J. Dong, Y. Ozaki and K. Nakashima, *J. Polym. Sci., Part B: Polym. Phys.*, 1997, **35**, 507–515.
57 J. Spěváček, M. Suchopárek and S. Al-Alawi, *Polymer*, 1995, **36**, 4125–4130.
58 C. Chang, D. D. Muccio and T. S. Pierre, *Macromolecules*, 1985, 2154–2157.
59 E. M. Woo and L. Chang, *Encyclopedia of Polymer Science and Technology*, American Cancer Society, 2011.
60 W. Kam, C.-W. Liew, J. Y. Lim and S. Ramesh, *Ionics*, 2014, **20**, 665–674.
61 I. C. McNeill and S. M. T. Sadeghi, *Polym. Degrad. Stab.*, 1990, **29**, 233–246.
62 H. L. Castricum, H. Yang, H. Bakker and J. H. Van Deursen, *Mater. Sci. Forum*, 1997, **235–238**, 211–216.
63 L. Aymard, C. Lenain, L. Courvoisier, F. Salver-Disma and J.-M. Tarascon, *J. Electrochem. Soc.*, 1999, **146**, 2015–2023.